RESEARCH ARTICLE | AUGUST 25 2023

An improved source of spin-polarized electrons based on spin exchange in optically pumped rubidium vapor FREE

K. J. Ahrendsen ; K. W. Trantham ; D. Tupa ; T. J. Gay

Rev Sci Instrum 94, 083308 (2023)
https://doi.org/10.1063/5.0149691

Review of Scientific Instruments ARTICLE pubs.aip.org/aip/rsi

An improved source of spin-polarized electrons based on spin exchange in optically pumped rubidium vapor

Cite as: Rev. Sci. Instrum. 94, 083308 (2023); doi: 10.1063/5.0149691
Submitted: 7 March 2023 • Accepted: 10 August 2023 •
Published Online: 25 August 2023

K. J. Ahrendsen,[1,a] K. W. Trantham,[2] D. Tupa,[3] and T. J. Gay[4]

AFFILIATIONS

[1] Jorgensen Hall, University of Nebraska, Lincoln, Nebraska 68588-0299, USA
[2] Physics Department, University of Nebraska-Kearney, Kearney, Nebraska 68849, USA
[3] Physics Division, Los Alamos National Laboratory, Los Alamos, New Mexico 87545, USA
[4] Physics Department, University of Nebraska-Lincoln, Lincoln, Nebraska 68588-0299, USA

[a] **Author to whom correspondence should be addressed:** kahrendsen@smith.edu

ABSTRACT

We have improved a polarized electron source in which unpolarized electrons undergo collisions with a mixture of buffer gas molecules and optically spin-polarized Rb atoms. With a nitrogen buffer gas, the source reliably provides spin polarization between 15% and 25% with beam currents >4 μA. Vacuum pump upgrades mitigate problems caused by denatured diffusion pump oil, leading to longer run times. A new differential pumping scheme allows the use of higher buffer gas pressures up to 800 mTorr. With a new optics layout, the Rb polarization is continuously monitored by a probe laser and improved pump laser power provides more constant high polarization. We have implemented an einzel lens to better control the energy of the electrons delivered to the target chamber and to preferentially select electron populations of higher polarization. The source is designed for studies of biologically relevant chiral molecule samples, which can poison photoemission-based GaAs polarized electron sources at very low partial pressures. It operates adjacent to a target chamber that rises to pressures as high as 10^{-4} Torr and has been implemented in a first experiment with chiral cysteine targets.

I. INTRODUCTION

This report describes in detail the third generation of a polarized electron source based on spin exchange between unpolarized electrons and optically pumped Rb atoms, which we call generically a "Rb spin filter." Its chief advantage over photoemission from negative electron affinity GaAs[1] is its ability to operate at relatively high background gas pressures and with targets that significantly degrade the performance of a GaAs source. It operates at typical pressures of 10^{-4} Torr, whereas GaAs sources generally require pressures below 10^{-10} Torr.

Recently, we observed a spin-dependent asymmetry in the destruction of the chiral molecule bromocamphor by polarized electrons through disassociative electron attachment (DEA).[2] These experiments constitute the first experimental evidence for preferential breakup of a chiral molecule by chiral electrons. Yet, because organic molecules easily poison GaAs photocathodes, the current standard source of polarized electrons, it would be technically challenging to gather enough data to broadly characterize the nature of this molecular destruction. The difficulties caused by contaminant molecules in the operation of GaAs sources have been noted in the literature.[3–5] Moreover, partial pressures of 10^{-11} Torr of organic molecules of the type we often study can deactivate a GaAs photocathode after only a few hours of operation.[6–8] We have been developing the source described here to be used in a series of experiments to measure polarized electron collisions with biologically relevant chiral targets.

The first generation of the Rb spin filter[9] could produce 4–5 μA of electron current with a spin polarization of 23%, but the unreliability of this prototype source made it unusable for extended experiments. The unpolarized electrons were produced by a cold cathode discharge, whose working gas, N_2, simultaneously served as a buffer gas to increase the efficiency of the optical pumping process. This shared-use method meant that any optimization of buffer gas pressure for the optical pumping process generally led to less-than-optimal electron production modes, eliminating the possibility

of careful systematic studies of buffer gas pressure to maximize the source's output polarization. The problem was exacerbated by the presence of a relatively high pressure of helium gas from the downstream He optical electron polarimeter. Another problem was that the cold-cathode discharge was usually unstable, leading to random fluctuations of both the output beam current and polarization, rendering the source unusable for systematic scientific experiments.

A second-generation source[10,11] decoupled the electron production mechanism from the optical pumping process. A simple heated filament emitted electrons thermionically, so the buffer gas pressure could be optimized for optical pumping. The buffer gas was also independent of the gas needed to measure the electron polarization. A laser beam counter-propagated along the electron beam axis to polarize the Rb vapor. This device produced 3 μA of current with polarizations that rarely exceeded 12% with nitrogen buffer gas but was much easier to operate. The relatively high pressure of buffer gas in the spin-exchange cell resulted in a source chamber operating pressure of ~10^{-4} Torr. This resulted in significant backstreaming of diffusion pump oil, which necessitated periodic cleaning of the electron transport optics and a strict upper limit of 200 mTorr buffer gas pressure. One trial run with ethene buffer gas managed to achieve an electron polarization of 23%. Unfortunately, longer runs with ethene left the entire source chamber coated with a thick film of heavily carbonized diffusion pump oil, which caused the electron transport optics to short out. Other operational problems arose from the poor temperature control of the Rb reservoir and the fact that the thermionic filament tended to droop into the optical pumping laser path at operating temperature, allowing only infrequent probe laser measurements of the Rb density and polarization.

This paper describes the recent improvements we have made to the Rb spin filter. The replacement of diffusion pumps with turbomolecular pumps has allowed us to investigate the use of buffer gases at much higher pressures than had previously been possible and to study the use of ethene and nitrogen as buffer gases more thoroughly. The Rb reservoir coupled to the spin-exchange cell is now heated using PID controller feedback. This simplifies operation and allows for a controlled cooldown process, which limits Rb buildup, resulting in longer run times for a single charge of Rb. A new optical pumping laser has higher power than its predecessor, which improves the output electron polarization, and a new thermionic filament design allows constant monitoring of the Rb density and polarization. The apparatus operation is now completely computer controlled, allowing much more efficient data taking. The addition of an einzel lens in the system improves both the beam transmission efficiency and narrows the energy width of the beam on target. All of these improvements are discussed in detail in the following. Taken together, they have resulted in a spin filter that is now a reliable source of polarized electrons that can be used in a variety of experiments; it has enabled us to make a study of chiral electron scattering from chiral molecules reliably and in a much shorter time than would have been required had we used a GaAs source.

II. APPARATUS OVERVIEW

The apparatus has three essential components: a source, beam transport section, and target chamber. As depicted in Fig. 1, the source chamber on the left is a 6-way 6 in. Conflat cross. This contains the Rb spin-exchange cell suspended at its center. The flange on its left houses electrical and gas feedthroughs and supports an electron gun. The right flange has a 3 mm-diameter knife-edge aperture leading into the differential pumping region. The two remaining flanges at the beam level have 6 in. windows for visual inspection of the system. The source chamber is pumped by a 300 l/s turbomolecular pump (Pfeiffer TPU 520). The entire vacuum system is depicted schematically in Fig. 2.

Referring again to Fig. 1, the Rb vapor is introduced into the spin-exchange cell (A) via a reservoir (B). The vapor can escape from the cell through two apertures that define the electron beam. These apertures also provide optical access for the pump and probe lasers, which are used to polarize and measure the polarization and number density of the Rb (see Sec. III).

A beam of electrons is produced by thermionic emission from a W filament placed 2 cm upstream of the spin-exchange cell. The beam is guided through the electron gun by a series of Davisson–Calbick apertures that are stacked on either side of the cell. Electron transport through the rest of the system is then managed primarily by the longitudinal magnetic field generated by the solenoidal magnets (C) on the exterior of the vacuum system.

The differential pumping region is made up of a 4.50–2.75 in. Conflat reducing cross with a bellows attached upstream and straight nipple downstream. The top flange leads to a four-way cross that supports the einzel lens system, electrical and mechanical feedthroughs for the einzel lens (D), and an ion gauge. An einzel lens allows for focusing or energy filtering of the beam, described in Sec. IV. The bottom flange leads to a Pfeiffer HiPace 80 turbo pump (67 l/s).

The target chamber at the right of Fig. 1 is constructed from a 8.00 in. Conflat nipple with a number of ports added at the beam level. The electrons enter through the 2.75 in. port on the left, travel through the chamber, and are collected in a Faraday cup (H) attached to the 1.33 in. flange on the right. Two additional 2.75 in. ports are centered at the same height as the first but rotated 54° clockwise and counterclockwise from the upstream port when looking from the top. They support an electrical feedthrough and a visual access port, respectively. At 30° anti-clockwise from the Faraday collector is an optical port for a helium fluorescence optical polarimeter (I) used to measure the polarization of the electron beam.[11] Two 2.75 in. Conflat ports on the top of the chamber are centered on the vertical plane that includes the electron transmission axis. They serve as the access for the target support assembly and as the mounting point for the He–electron polarimeter cylinder (G). The polarimeter cylinder is used to define a uniform potential for the electron–He collision volume. It has a secondary function of inhibiting diffusion of the He gas throughout the vacuum chamber by directing it to the pump below. On the centerline of this cylinder is a needle tip used to admit He to the system just above the electron beam. A 1.33 in. Conflat port connects both an electrical feedthrough and an ion gauge to the system through a tee. The target chamber is pumped by a Pfeiffer HiPace 700M turbomolecular pump (685 l/s).

The ability to toggle between experimental collision targets and the polarimeter and Faraday cup is provided by a trochoidal electron deflector[12] (E). When a horizontal electric field is applied at the deflector plates, the beam is steered vertically away from the transmission axis and on a path to the experimental targets (F), located just below the transmission axis (see Sec. V).

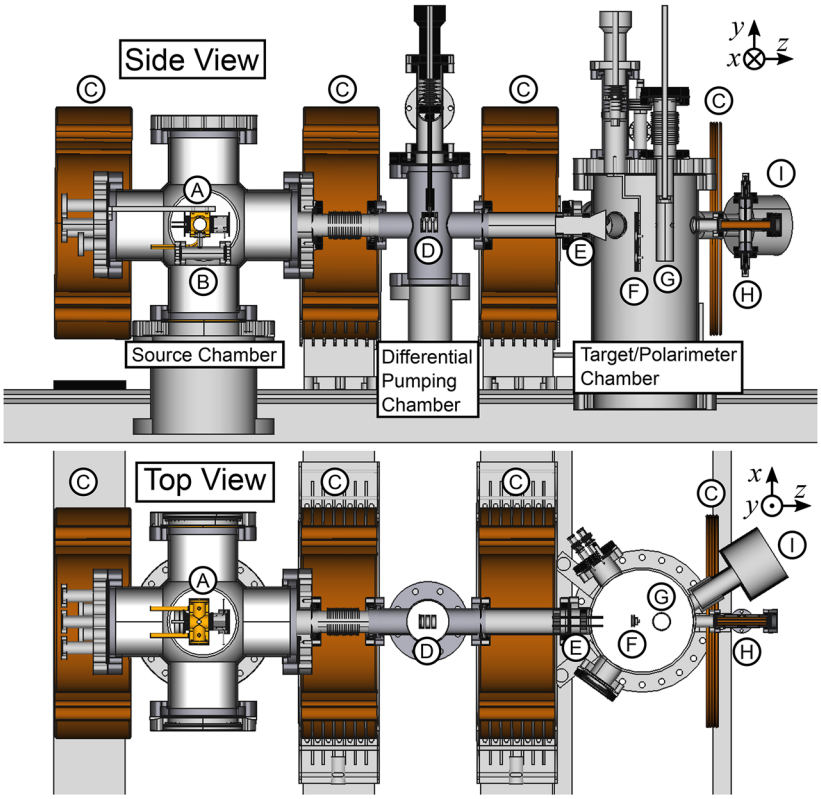

FIG. 1. Two views of the Rb Spin Filter apparatus. On the left is the source chamber where polarized electrons are produced through spin-exchange interactions of unpolarized electrons with polarized rubidium. On the right is the target/polarimeter chamber where the electron beam polarization is measured and the experimental targets are mounted. The center differential pumping chamber isolates the two chambers' process gases from each other and provides additional controls for manipulation of the beam. See the text for a full description of the labeled components.

Many aspects of the control of the apparatus have been automated through the use of a home-built data acquisition system controlled by a Raspberry Pi. The system uses a RS-485 data transmission line as its backbone because it allows for signal transmission over longer distances than those used in GPIB or RS-232 protocols. Connected to this line are a number of devices for either interfacing with existing electronics or providing controls to motors to automate actions related to the optics of the system: blocking and redirecting lasers and rotating optical elements. All the materials needed to assemble such a system are described in our public code repository hosted on GitHub.[13]

III. RUBIDIUM CONTROL

We polarize the electron beam in our system via spin exchange with optically pumped polarized rubidium atoms. Rubidium vapor is introduced into the spin-exchange chamber by heating the Rb reservoir, a modified 1.33 in. Conflat nipple containing an opened 1 g breakseal glass vial of Rb. When warming the reservoir, it is essential to maintain the temperature of the spin-exchange cell at least 30 °C above that of the reservoir. This prevents the vapor from condensing on the components of the electron gun and increases the length of time over which the system can be operated without cleaning. Two cartridge heaters are bound by wire to the exterior of the reservoir, and another set of heaters are embedded in the copper block from which the spin-exchange cell is made. The heaters for the spin-exchange cell and the rubidium reservoir are powered by a single variable AC power supply operated at about 70 V and controlled by two temperature controllers (Omega CN7500), which use pulse-width modulation to vary power delivery through a pair of solid-state relays (Crydom D4825-5595). Type-K thermocouples monitor the reservoir and cell temperatures to provide the necessary feedback for the temperature controllers. Before the implementation of the temperature controllers, rubidium oxide buildup was a frequent problem in maintaining operation of the spin filter. With the temperature controllers, particularly during the reservoir cooldown process, the amount of oxide buildup is significantly reduced to the point that the system can use two charges of Rb before requiring a cleaning. A 1 g charge of Rb will last roughly 40 hours when the spin filter is running with nominal high-temperature heating of the reservoir and spin-exchange cell.

The Rb is polarized by a circularly polarized pump laser, while a probe laser is used to measure both the density and polarization of

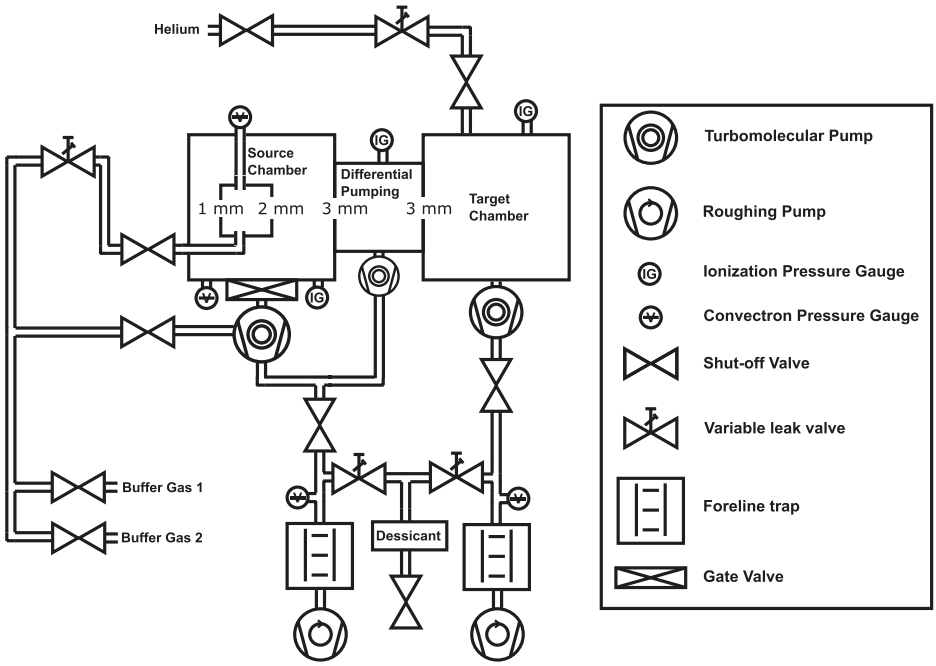

FIG. 2. A schematic of the vacuum system. The vacuum chamber is evacuated by three turbomolecular pumps. The target chamber turbopump is backed by a single roughing pump, while a second pump serves as the backing pump for both the source and differential pumping turbos. The buffer gas, used for obtaining higher Rb polarizations, and the helium gas, used for determining the electron polarization, are delivered as indicated. Electron beam aperture sizes are indicated at the interfaces of each of the chambers.

the vapor. The layout of the lasers and optics is shown schematically in Fig. 3. The probe laser (Sacher Lasertechnik Cheetah, 795 nm) produces up to 35 mW of power, but we typically operate it at less than 1 mW. The probe laser beam first encounters an optical isolator to protect it from back reflections and the pump beam. A microscope slide then samples the beam where the redirected portion is sent to a wavemeter (HighFinesse WS6-200). A computer controlled beam block allows for toggling the laser on and off without altering the drive current. Next is a linear polarizer (LP) to clean up the laser's linear polarization and allow for additional attenuation. A 90/10 beamsplitter follows, and the lower intensity redirected beam passes through a Rb vapor reference cell. This is used as a physical standard against which the output of the wavemeter can be compared. The final element the probe beam encounters before entering the vacuum chamber is an optical chopper. The pump laser's intensity is much higher than that of the probe laser, and the signal from the probe laser can be modulated to allow for isolation of its signal using a lock-in amplifier (SRS 830). The probe beam is analyzed by a half-wave plate (HWP) followed by a polarizing beam splitting cube monitored by two photodiodes (PD). The position of the HWP is computer controlled. Typically, the linear polarization of the probe beam is determined from a discrete Fourier transform of the PD signals for equally spaced rotation angles of the HWP.

We measure the Rb number density n_{Rb} using the Faraday rotation of near-resonant light as described by Wu *et al.*[14] The azimuthal angle of vibration of the linearly polarized probe laser is measured at six frequencies between −30 and +30 GHz detuning, referenced to the D1 line center of the rubidium profile,[15] 377.107 THz, and fit to the function

$$\bar{\theta}(\nu) = \frac{A_2 \nu_o^2 \nu^2}{c^2(\nu - \nu_o)^2} + \frac{A_4 \nu_o^2 \nu^2}{c^4(\nu - \nu_o)^4}, \quad (1)$$

where ν is the frequency of the probe laser, ν_o is the line-center frequency, c is the speed of light, and A_2 and A_4 are fitting parameters. The number density n_{Rb} can then be determined from the value of the fitting parameter A_2 by the relationship

$$n_{Rb} = \frac{2\nu_o h}{r_e f_{ge} \kappa \mu} \frac{A_2}{\int B \cdot d\ell}, \quad (2)$$

where r_e is the classical radius of the electron, f_{ge} is the transition strength, $\kappa = 4/3$, μ is the Bohr magneton, and $\int B \cdot d\ell$ is the magnetic field integrated over the length of the spin-exchange cell. Although this formula is used in Wu *et al.*'s original paper for much thicker vapors and larger detunings than those used here, we find the calculated densities to be in good agreement with the values calculated by optical absorption methods at densities where both measurements are possible. An example of the collected data and fit is shown in Fig. 4.

The pump laser is a TOPTICA TA pro laser system tuned to a frequency of +1.5 GHz from the line center of the Rb D1 transition. A small fraction of the light from the pump beam is picked off inside the laser housing for wavemeter and spectrum analyzer diagnostics. A beamsplitter further reduces the intensity of the refer-

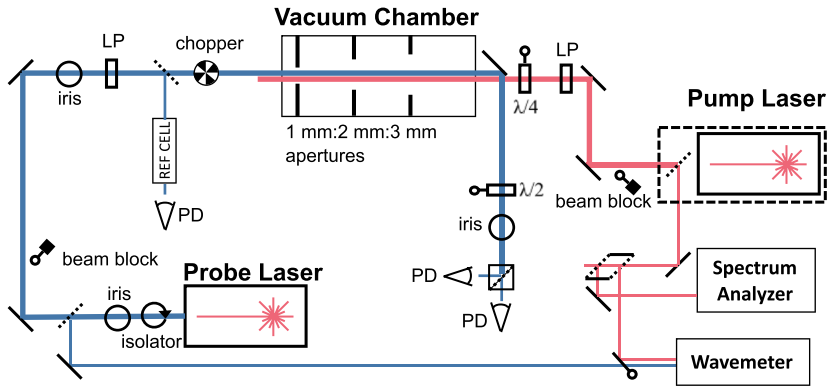

FIG. 3. A schematic of the optics used to optically pump Rb and to measure its density and polarization. The small circles connected to various optical elements indicate that they are computer controlled. LP = linear polarizer, $\lambda/4$ = quarter-wave plate, $\lambda/2$ = half-wave plate, and PD = photodiode.

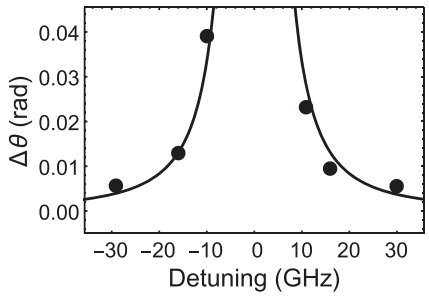

FIG. 4. Typical data collected to measure the Rb number density. As the detuning approaches zero, the polarization angle of the probe laser (θ) shifts. Angles are measured at six detuning frequencies (data points) and fit to Eq. (1) (solid line). The calculated number density for this dataset is $3.7(7) \times 10^{12}$ cm^{-3}.

ence beam for input into the wavemeter. A computer controlled flip mirror toggles between measuring the pump and probe beam during automated analysis. A Glan-Thompson linear polarizer cleans up the laser polarization, followed by a quarter-wave plate (QWP) to circularly polarize the beam. The wave plate positions for maximum circular polarization are determined by back-reflecting the beam through the circular polarizer and finding a minimum intensity in the reflected beam. We measure the beam to be 99.75(7)% polarized.

We also measure the Rb polarization P_{Rb} with Faraday rotation methods. The probe laser rotation is collected with the pump laser set to each helicity of circularly polarized light. The difference between the pump-light data and the no-pump-light data gives the angle of rotation solely due to the polarization of the Rb vapor: the paramagnetic Faraday rotation. This angle is proportional to the polarization,[16]

$$P_{Rb} = \frac{-4}{r_e c f_{ge}} \frac{\delta_{pr} \Delta\theta}{L n_{Rb}}, \tag{3}$$

where δ_{pr} is the detuning of the probe laser (in Hz), $\Delta\theta$ is the probe beam's rotation angle, and L is the path length of the laser through the vapor.

We determine the optimum frequency for polarizing Rb by scanning the pump laser over its absorption profile in 0.5 GHz increments and measuring the rotation of the probe laser at each step. The largest rotation of the probe polarization identifies the optimal pump frequency. Such data are shown in Fig. 5. We observe the same "spin reversal phenomena" originally reported by Norrgard *et al.*[17] although reduced in magnitude. The spin reversal occurs because of small components of linearly polarized light in the pump beam. The electron polarization P_e also flips sign where we observe the Rb spin reversal. Rotating the QWP from its optimal position results in large changes in P_{Rb} and associated changes in the electron polarization. We find that 1 W of laser power, the power at which we typically use in the experiment, is sufficient to saturate the Rb polarization, as can be seen in Fig. 6. The error bars for the data collected in this figure are comparatively larger than those in Fig. 5 because of a higher uncertainty in n_{Rb}; for these data, only two measurements were used to determine the density while the former used seven. Figure 6 also shows that the magnitude of the maximum attainable polarization depends on the pump helicity. This asymmetry was associated with the direction of the magnetic field; reversing the field resulted in the opposite polarization being larger. Both the electron polarization and the Rb polarization had this asymmetry, indicating that it was not a measurement error. Although we do not currently understand its cause, we addressed the issue by normalizing our results by the magnitude of the electron polarization in the experiment described in Sec. VII.

The buffer gas is introduced into the spin-exchange cell through a 5 mm inner diameter tube. Another 5 mm-diameter tube is used to monitor the cell's pressure. The buffer gas increases the maximum polarization attainable by quenching the excited Rb state before depolarizing radiation is emitted.[9,18] It also influences the rubidium densities we obtain for a given reservoir temperature. Studies of how P_{Rb} varied with buffer gas pressure $\mathcal{P}_{BG}$ were difficult as n_{Rb} cannot easily be held constant as $\mathcal{P}_{BG}$ is varied. The effect the variation of $\mathcal{P}_{BG}$ had on n_{Rb} is illustrated in Fig. 7. Such effects occur because the system is not sealed; buffer gas streams through the apertures of the spin-exchange cell, carrying Rb with it. The $\mathcal{P}_{BG}$ value is usually high enough to result in a viscous flow, which scales linearly with pressure. Although n_{Rb} on its own is not sufficiently

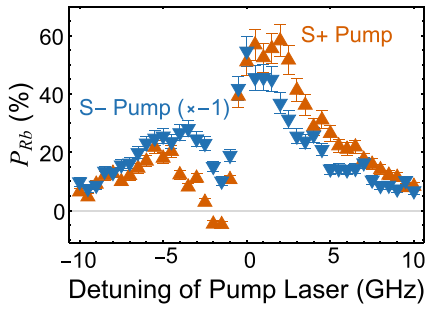

FIG. 5. The relationship between the pump laser frequency and rubidium polarization, P_{Rb}. The highest magnitude of polarization was obtained at 1.5 GHz with S+ pump light, so this was the frequency used to generate spin-polarized electrons. We observe the spin reversal phenomenon[17] at ∼−1.5 GHz; the magnitude is smaller than that has been observed previously, indicating that we have purer circular light polarization.

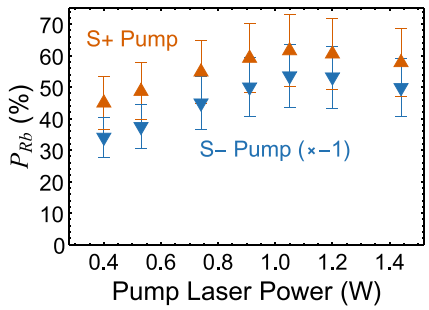

FIG. 6. Rubidium polarization P_{Rb} vs laser power for both helicities of pump light. We observe that the polarization saturates at ∼1 W of laser power. The data were collected with 330 mTorr of N_2 buffer gas and a pump laser detuning of +1.5 GHz.

high to produce viscous flow, collisions with the buffer gas molecules increase the Rb flow rate from the cell with an increase in buffer gas pressure. This rate is significant when compared to the flow rate in the Rb reservoir, so we see n_{Rb} drop with an increase in $\mathcal{P}_{BG}$.

IV. BEAM TRANSPORT

The initially unpolarized electrons are generated by thermionic emission from a W filament. In the second generation Rb spin filter, a standard filament of circular cross section would often shift in position as it warmed, blocking optical access of the probe laser to the spin-exchange cell. We solved this problem with a single turn helical filament from a tungsten ribbon wire (0.002 in. thick and 0.025 in. wide). With the new configuration, the single helical turn stays in its initially mounted position even after warming. The electrons emitted from the W are formed into a beam by a series of electrode apertures immediately downstream from the filament and then guided into the spin-exchange cell. We refer to the filament and these electrodes collectively as the "electron gun," which is shown in Fig. 8. Table I lists typical voltages supplied to each element that resulted in good electron transmission.

The electron beam passes through the spin-exchange cell aided by a longitudinal electric field produced by the electrodes on either

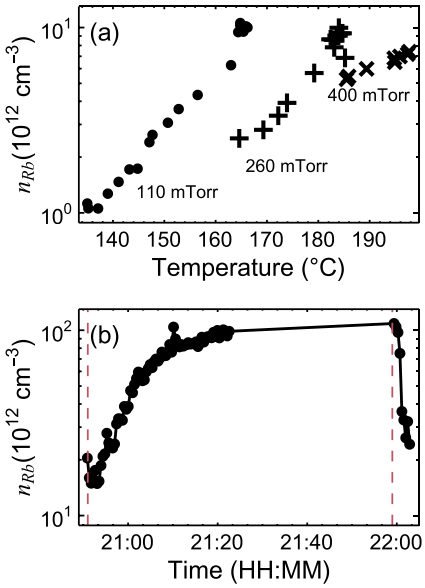

FIG. 7. (a) The interaction between $\mathcal{P}_{BG}$ and n_{Rb} as the reservoir temperature is varied. (b) Rb density in the spin-exchange cell vs time as $\mathcal{P}_{BG}$ is adjusted. The vertical dashed lines indicate when $\mathcal{P}_{BG}$ is changed; the line on the left corresponds to an abrupt drop from 400 to 130 mTorr, while the one on the right indicates an increase back up to 400 mTorr. The solid line is drawn to guide the eye.

end (1D and 2A) and a longitudinal magnetic field to be discussed later. The electric field is important because it continues to push the electron beam downstream after a significant fraction of its electrons have thermalized in the buffer gas. After passing through the cell and becoming polarized, the beam is again guided and focused by a series of electrodes through a 3 mm grounded aperture leading to the differential pumping chamber. The differential pumping chamber has a retractable einzel lens in its center which is essential for achieving efficient transport through the system when the electrons have kinetic energy below 10 eV.

The electron transport through the system is primarily achieved by a longitudinal magnetic field generated by a series of three concentric "double coil" electromagnets (C in Fig. 1) and one single coil "hoop" magnet (on the far right of Fig. 1). The double coil magnets consist of a first coil with ID = 8.0 in. and OD = 8.8 in., which is 3 in. long, and a second coil with ID = 9.4 in., OD = 10.2 in., and also 3 in. long. This design with two separate coils is meant to facilitate air cooling. These compound coils are driven with a current of 3 A, generating a magnetic field of 0.02 T at their center. The hoop magnet is driven at 2.5 A and produces a field of 0.002 T at its center. The combined magnets produce a field similar to that shown in Fig. 9. This magnetic field is particularly important to guide the electrons through the spin-exchange cell, where collisions with the buffer gas would otherwise cause the incident electrons to diffuse away from the beam axis. The magnitude of the magnetic field on the axis of the apparatus varies along its length. The efficiency of the optical pumping depends upon the parallelism between the magnetic field and the pump laser beam where they overlap in the spin-exchange cell but does not vary much with the magnitude of the field. In this

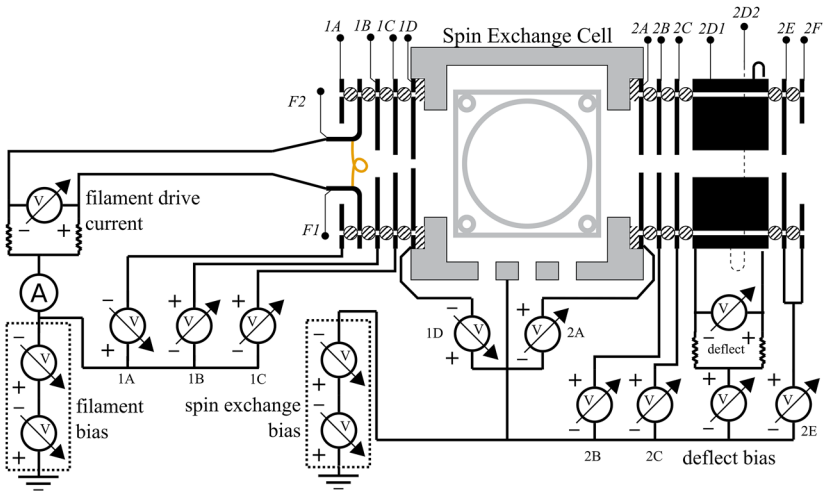

FIG. 8. A schematic of the electron gun and its electrical controls. The inner diameter of the spin-exchange cell is 2 cm. Each electrode is isolated by sapphire balls or, if the electrode is adjacent to the spin-exchange cell, a Kapton sheet. These insulating materials are indicated with a striped pattern. The filament that generates the spin-polarized electrons is a single loop, which encircles the transmission axis of the system. In the longitudinal magnetic field of the apparatus, the deflection electrodes 2D1 and 2D2 produce a beam drift perpendicular to the transverse field.

TABLE I. Typical source voltages for optimal electron transmission. The filament drive current was usually held at 4.0 A when Rb was in the system and 4.2 A when Rb was absent.

Element (Fig. 8)	Voltage
Filament bias	240
1A	4.0
1B	33.0
1C	12.8
Spin-exchange cell	140
1D	2.0
2A	0.0
2B	120
2C	120
Deflect center	120
Deflection	0.0
2E	120

region of overlap, the paraxial B-field deviates by less than 2° from the pump laser path, which will not appreciably lower the optical pumping efficiency in the spin-exchange cell.

V. BEAM TARGETS

The electron beam's polarization P_e is measured using a He optical electron polarimeter in the target chamber (Fig. 1). The polarimeter design is described in detail in a previous publication.[11] The incident longitudinally polarized electrons excite the 388.9 nm $3^3P \longrightarrow 2^3S$ transition in He, and the polarization of this fluorescence can be related to the electron polarization through the relation,

$$P_e = \left(\frac{1.685P_3}{0.714 + 0.982P_1}\right), \tag{4}$$

where P_1 is the relative Stokes parameter describing the horizontal and vertical linear fluorescence polarization and P_3 is the relative Stokes parameter for circularly polarized light.

We improved the polarimeter for this work with a better vacuum system and by placing the detector at a smaller angle relative to the transmission axis, increasing its sensitivity to circularly polarized light by 4% and resulting in the updated relationship shown in Eq. (4). The Stokes parameters are determined using the method described by Berry *et al.*[19] A QWP is rotated through a full revolution, which modulates the intensity of the transmitted light. The intensity as a function of the waveplate position is converted into frequency space, and the amplitudes of certain frequencies can be related to the Stokes parameters.

A thin-walled steel tube of diameter 1.27 cm surrounds a steel capillary (i.d. = 0.8 mm), which injects helium gas into the system to form a plume of target gas with maximum density on the beamline. The tube creates a uniform potential for the e^-–He interaction region and enables a rudimentary retarding field analysis of the beam to study its energy distribution (to be discussed further in the following). Downstream from this tube is the Faraday cup where the final transmitted electron current is measured.

Because our apparatus requires uninterrupted optical access for the pump laser along the electron beam path, there must be a mechanism for diverting the beam to the off-axis experimental targets. The longitudinal B-field parallel to the electron propagation axis makes a trochoidal monochromator-like device a natural choice to deflect the electron beam vertically. When an electric field is applied perpendicular to the magnetic field, the resulting motion of the beam

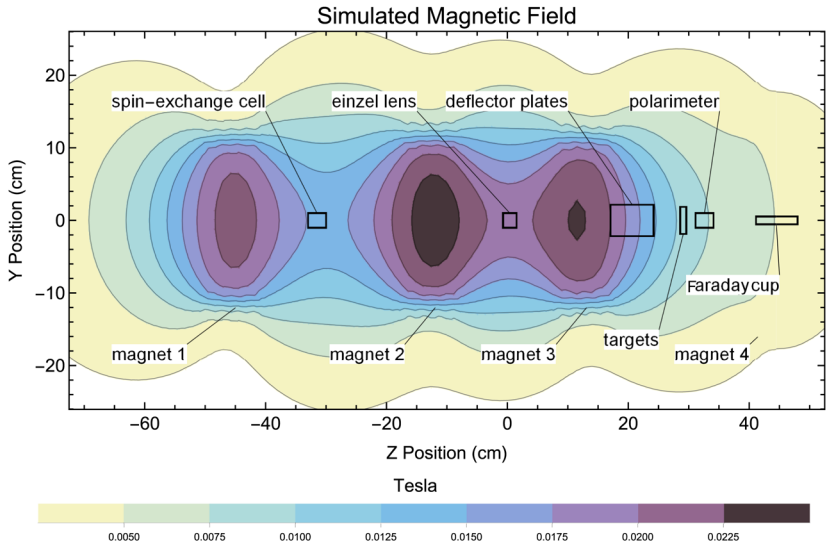

FIG. 9. A model of the Z-component of the calculated magnetic field throughout the apparatus. The positions of various components of the apparatus are indicated.

center is a drift in the direction of $\mathbf{E} \times \mathbf{B}$. Thus, by applying a voltage to parallel plates (Fig. 1, element E), we can divert the beam by 1.5 cm to a path incident on the experimental target.

The carriage system we use to hold the experimental targets (Item F in Fig. 1) has two positions and is mounted on a linear motion feedthrough to allow selection of the targets. The targets themselves are electrically isolated from the clamping frames by thin rings of the Kapton sheet placed on both their front and back faces.

The energy distribution of the electron beam was studied by taking a retarding field spectrum; we measured the current transmitted to the Faraday cup as a function of the He target cylinder voltage. The derivative of this value gives the energy spectrum of the beam emerging from the source chamber (Fig. 10). The energy distribution depends on the source filament voltage, the buffer gas pressure, the potential of the Rb spin-exchange cell (−40 V for the data in Fig. 10), and, to a lesser degree, the voltages on the electrostatic elements 2A–2 F shown in Fig. 8. It is also affected in a detailed way by the energy dependence of the various collision channels for e^-–N_2 scattering. The difference between the filament bias and the spin-exchange cell bias determines E_i, the kinetic energy of the unpolarized electrons incident on the Rb/buffer gas target. When there is no buffer gas in the system, the electron's energy is essentially determined by the voltage of the filament [Fig. 10(a)]. We interpret the order and shape of the curves in Figs. 10(b) and 10(c) with an understanding of the interactions between the electrons and the nitrogen buffer gas. With as little as 100 mTorr of buffer gas in the spin-exchange cell, an interesting reordering of the output energies for the various E_i values occurs. Now, the output electron beam when E_i = 100 eV (corresponding to a filament voltage of −140 V) has the lowest value, about 37 eV, with increasing output energies for E_i = 60, 30, 20, and 14 eV. (The E_i = 8 eV peak has roughly the same energy as that of the E_i = 20 eV peak.) Similar peak positions occur when the buffer gas pressure is raised to 400 mTorr [Fig. 10(c)] although the output energies are now all lower with broader energy spreads. This ordering reversal and energy broadening of the transmitted electron beam is largely the result of three collision channels: N_2 ionization (17 eV threshold with a cross section maximum at 100 eV), impact excitation of N_2 electronic states (11 eV threshold), and N_2 vibrational mode excitation (cross section maximum at ~2.5 eV). At both buffer gas pressure studied, the incident electrons are strongly thermalized by inelastic scattering processes. As E_i increases above the N_2 ionization threshold, the electrons from the ionization process having small kinetic energies are added to the beam, but the only inelastic channel in which they can participate is vibrational mode excitation. The output electron beam for E_i = 100 eV comprises many low-energy secondaries and a few primaries that have undergone large energy losses, which subsequently lose even more energy due to inelastic vibrational collisions with buffer gas both inside and downstream from the spin-exchange cell. This secondary electron energy loss also accounts for the E_i = 60 eV peak. Electrons with E_i = 30 eV and below will be much less effective at producing low-energy secondaries due to ionization and will also have relatively small cross sections for N_2 electronic-state excitation. They will thus thermalize less efficiently and will only lose small amounts of energy in N_2 vibrational excitation. A notable exception here is the E_i = 14 eV peak at 100 mTorr for which primary electrons are transmitted largely without energy loss, giving this beam the highest output energy. This is the result of their energy being very low to ionize N_2 or effectively excite its electronic state, but very high to excite effectively N_2 vibrational modes. Thus, they are poorly thermalized.

VI. RESULTS

The source has been thoroughly tested to reliably produce $P_e \geq 15\%$ with ~300 nA at 140(2) eV. (We limited the current to 300 nA due to the physical constraints of our target; the source is capable of producing much more.) The system has also produced

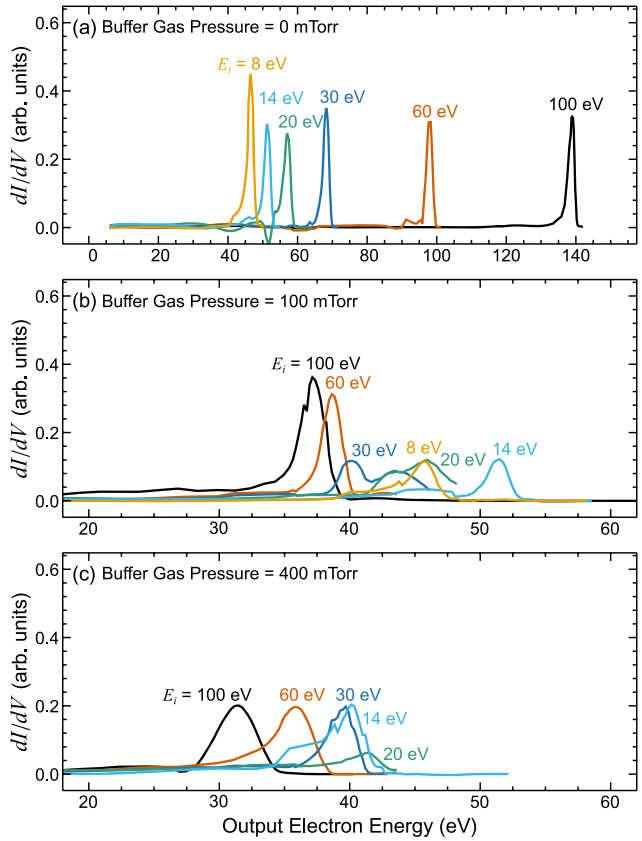

FIG. 10. Retarding field curve derivatives. This series of figures illustrates the effect the buffer gas has on the energy of the transmitted electrons. Each panel represents data collected at a fixed buffer gas pressure and contains multiple sets at different incident electron energies E_i, which label the curves. Note the different horizontal scales for (a). (a) With no buffer gas, the electrons have an energy that corresponds to the filament voltage. (b) At $\mathcal{P}_{BG}$ = 100 mTorr, almost all of the electrons will interact multiple times with N_2 and Rb in the spin-exchange cell, giving them very low kinetic energy at the cell potential −40 V in these data. (c) At $\mathcal{P}_{BG}$ = 400 mTorr, the electron energy distribution is significantly broadened and slowed because of the increased number of energy-loss collisions downstream from the spin-exchange cell but prior to the differential pumping chamber (see the text).

4 μA with P_e = 15% and shows no indication of smaller values of P_e at higher currents (see Fig. 11). Higher polarizations up to 25% are maintained through precise alignment of the vacuum apertures and the longitudinal B-field. The current typically drifted during the course of measurements at a rate of 5% of its initial value over 15 min. These variations are primarily due to thermally induced mechanical fluctuations of the thermionic filament relative to the electron gun optics. The output current of the source is limited by the lifetime of the filament. For the ~300 nA we used in our experiments, the filament never burned out, lasting for over 80 h of data collection. We believe it could last much longer, but it was regularly replaced during the course of routine cleaning.

The polarization of the output beam P_e is measured using Eq. (4). However, the relation between P_3 and P_e described by Eq. (4)

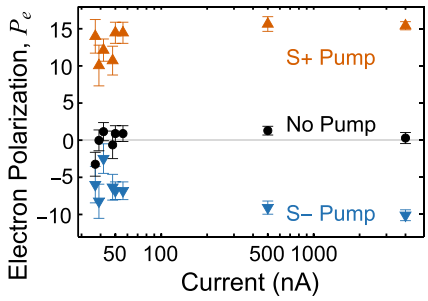

FIG. 11. Electron polarization, P_e, as a function of output current. These data were collected with 400 mTorr of N_2 at an electron beam energy of 140 eV.

is strictly valid for energies within 0.6 eV of the 3^3P 23.0 eV excitation threshold.[20] The 389 nm fluorescence signal increases rapidly above 23.0 eV, but above 23.6 eV, cascading from the 4^3S and higher levels can contaminate the polarization signal. This contamination must be balanced with the need for a useable intensity of light. Figure 12 shows both the light intensity and its P_3 polarization as a function of electron energy.

An important improvement in the operation of the spin filter resulted from the replacement of the diffusion pump on the source chamber with a turbomolecular pump. Although the 300 l/s pumping speed of the Pfeiffer TPU 520M is significantly lower than the 700 l/s diffusion pump it replaced, we found it eliminated the pump-oil backstreaming problem, which plagued earlier iterations of the apparatus and allowed us run the source at buffer gas densities of 800 mTorr—much higher than the 200 mTorr permitted by the diffusion pump. We could thus systematically explore a broader range of buffer gas densities (200 mTorr < $\mathcal{P}_{BG}$ < 800 mTorr) to optimize the performance of the spin filter using the "spin transfer efficiency"

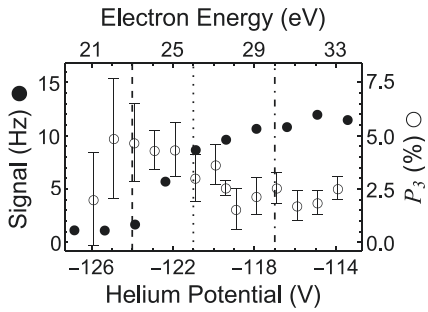

FIG. 12. Energy dependence of the P_3 Stokes parameter with $S-$ pump light. The filled data points show the single photon count-rate signal (in Hz or counts per second) from the 389 nm fluorescence intensity, which has an onset of 23.0 eV, thus setting the upper axis scale. The right axis shows the scale for the P_3 Stokes parameter indicated by the open circles. The lines represent the excitation function onset (dashed line), the higher electron energy at which P_e was determined in earlier data runs (dotted-dashed line), and the lower value of the electron energy at which P_e was determined for recent data runs (dotted line).

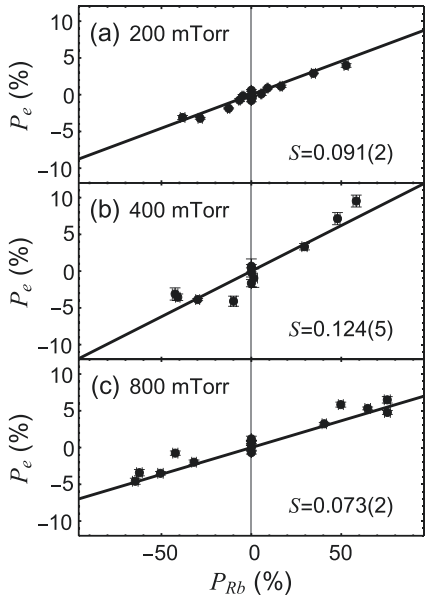

FIG. 13. (a)–(c) A measurement of the spin transfer efficiency S for N_2 buffer gas pressures of 200, 400, and 800 mTorr. The electron polarization P_e vs P_{Rb} with $n_{Rb} = 10 \times 10^{12}$ cm^{-3} is plotted as the pump laser is tuned off resonance to vary P_{Rb}. The slope of a linear fit fixed through the origin gives the value of S. For each of these runs, the energy of the electrons incident on the Rb, E_i, was 100 eV.

S as our figure of merit. The spin transfer efficiency is the value of the linear slope relating P_{Rb} to P_e,

$$S = \frac{\Delta P_e}{\Delta P_{Rb}}. \tag{5}$$

Measuring this value allowed us to study the spin transfer mechanism in addition to searching for a maximum polarization.

The data for S values for different values of $\mathcal{P}_{BG}$ with N_2 at $n_{Rb} = 10 \times 10^{12}$ cm^{-3} are shown in Fig. 13. Although increasing $\mathcal{P}_{BG}$ always brought a rise in P_{Rb}, it did not always increase P_e. We see that the buffer gas may have a depolarizing effect on electrons transmitted through the spin-exchange cell. This result is surprising because spin is not expected to be significantly affected by low-energy elastic collisions with N_2 ground-state molecules.

In Fig. 14, we show how S varies with respect to n_{Rb} for three different values of $\mathcal{P}_{BG}$ and with both N_2 and ethene buffer gas. Prior iterations of the spin filter operating at 200 mTorr investigated a total of four types of buffer gas and saw the highest spin polarizations using ethene and the second highest with nitrogen.[10] At low buffer gas pressures, we again see that ethene outperforms N_2, but at 400 mTorr, nitrogen has a slightly larger value of S. We attempted to collect data with 800 mTorr of ethene in the system but found that the laser windows rapidly became opaque. Nitrogen did not exhibit this contaminating effect, so we used it for the remainder of the studies.

We found minimal variation in S when adjusting n_{Rb}. This was unexpected, given that increasing the density by an order of magnitude should produce ten times more collisions with spin-polarized rubidium atoms. Based on these data, there appears to be an optimal

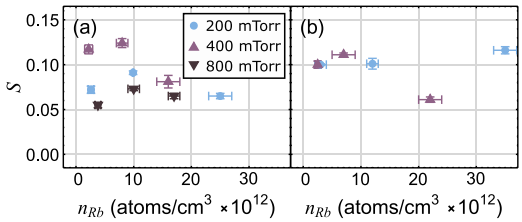

FIG. 14. A summary of S values as a function of n_{Rb} and $\mathcal{P}_{BG}$. (a) was collected using N_2 as a buffer gas, and (b) was collected using ethene.

zone for both $\mathcal{P}_{BG}$ and n_{Rb} that maximizes the transfer of Rb polarization to electron polarization: ($\mathcal{P}_{BG}(N_2)$ = 400 mTorr; $n_{Rb} = 10^{13}$ cm^{-3}).

These initial investigations of source performance were performed before the addition of the new target chamber but after the differential pumping section used in Ref. 10 had been removed in a failed attempt to simplify the apparatus and improve its electron beam transmission efficiency. After finding that the optimal value of $\mathcal{P}_{BG}$ was a factor of two to three higher than what had been previously used in the system, we re-introduced a differential pumping stage between the source and the new target chamber to ensure isolation of the two process gases.

A differential pumping section provides an additional benefit of space to add an einzel lens to better adjust and control the electron beam. The einzel lens is essential at electron beam energies below 10 eV to achieve transport through the vacuum chamber but at higher electron energies has little effect on the transport efficiency. However, at higher energies, it is valuable as an energy filter for the electron beam. At $\mathcal{P}_{BG}$ = 400 mTorr, most of the electrons exiting the spin-exchange cell have lost almost all of the kinetic energy they had just before entering the cell [Fig. 10(c)]. However, because the target cell and the last electrodes (2E and 2F) have negative voltages during normal electron gun operation, these electrons continue to gain kinetic energy as they accelerate toward the grounded exit aperture of the source chamber. These accelerated electrons have a significant probability of undergoing additional energy-loss collisions before reaching the differential pumping chamber due to the relatively high buffer gas pressure at which we now operate. Biasing the entire einzel lens stack with a negative voltage enabled us to reject lower energy electrons from the beam generated by such collisions and thus narrow the beam's energy spread on the target. This can be seen from the retarding field curve shown in Fig. 15.

Our retarding field analysis provides evidence that electrons may experience a significant number of collisions with buffer gas between the spin-exchange cell and the differential pumping region. Our spin transfer measurements hint that there may be some electron polarization loss in collisions with buffer gas. We speculate that electrons in the low-energy tail may have reduced polarization, but these electrons can be rejected by the einzel lens.

Previously, we had been measuring the electron polarization near the peak of the excitation function since this provided the largest intensity of light. Subsequently, we collected the data shown in Fig. 12 and verified that an electron energy closer to threshold would provide a more accurate polarization measurement. Measuring P_e closer to threshold, we retook the data to determine a spin

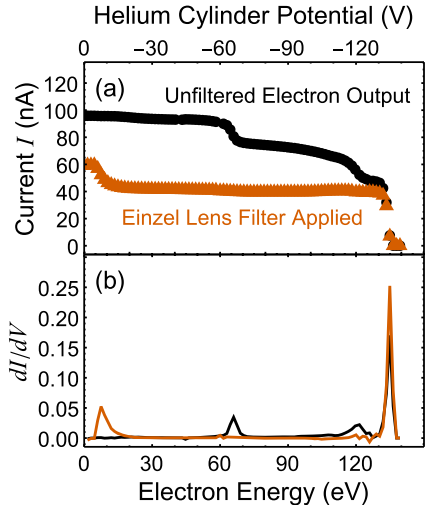

FIG. 15. (a) Retarding field spectra with $\mathcal{P}_{BG}$ = 400 mTorr of N_2, showing how a negative voltage on the einzel lens makes our electron beam more monoenergetic. The lower energy electrons, evident in the rapid increases in the retarding field spectra at about −120 and −70 V when the energy filtering is turned off, are produced by collisions with background buffer gas outside of the spin-exchange cell region. (b) shows the derivative of part (a). These lower energy electrons were not present in earlier versions of the Rb spin filter because we were operating at much lower values of $\mathcal{P}_{BG}$.[10]

transfer function under optimal conditions of $\mathcal{P}_{BG}$ = 400 mTorr and n_{Rb} = 7.8(1) × 10^{12} cm^{-3}. Figure 16 shows the results, which give a significantly higher value of S of 0.24.

Selecting the optimal buffer gas pressure and n_{Rb} with a careful retuning and aligning of the apparatus, we consistently measure electron polarizations over 20% for E_i = 140 eV. These data are shown in Fig. 17. This achievement is particularly notable because the system is able to cycle between vacuum and atmosphere for Rb reloading and is ready to produce spin-polarized electrons at its working vacuum in less than 12 h. A typical GaAs source must undergo a bakeout and activation procedure, which would render the system unable to produce spin-polarized electrons for at least 96 h. There is significant improvement of the spin filter's operational

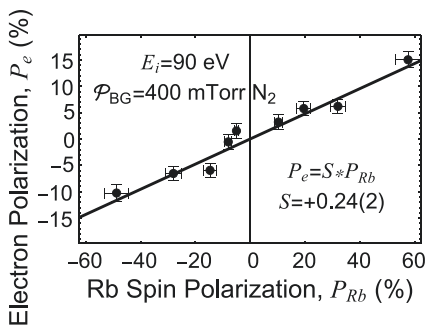

FIG. 16. A spin transfer efficiency curve collected at E_i = 90 eV. The polarized electrons strike the He target 3 eV above the excitation threshold (see Fig. 12).

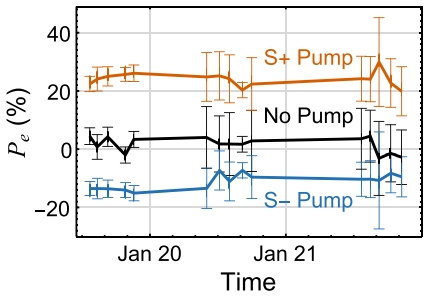

FIG. 17. Electron polarization P_e taken over the course of several days; these data were collected with E_i = 100 eV, $\mathcal{P}_{BG}$ = 400 mTorr N_2, and n_{Rb} = 5 ×10^{12} cm^{-3}. The current of the electron beam was ~300 nA.

consistency in the newly accessible vicinity of $\mathcal{P}_{BG}$ = 400 mTorr compared to the previous typical $\mathcal{P}_{BG}$ of 130 mTorr.

After identifying the proper energy at which to measure P_e and with 400 mTorr of nitrogen as a buffer gas, we were able to obtain greater than 10% electron polarization at nearly all values of E_i between 5 and 100 eV. Figure 18 shows the dependence of extracted current and P_e as a function of E_i for buffer gas pressures of both 130 mTorr (that used in Ref. 10) and 400 mTorr. This indicates a marked improvement of the new spin filter over the previous version.[10] The current dataset at 130 mTorr and that of Ref. 10 are qualitatively similar with the exception of the extracted electron current below E_i = 15 eV. This is likely due to the significantly different structure of our new thermionic filaments and their effect on the spin-exchange cell's input electron optics. Above 15 eV, however, I increases steadily in both Ref. 10 and this work, the result of the increasing number of electrons produced by impact ionization of the N_2 buffer gas; the electron-impact ionization cross section for N_2 has a maximum at E_i = 100 eV.[21] The advantage of increased buffer gas pressure for the production of higher P_e is seen clearly in Fig. 18(b). The initial decrease in P_e as E_i is increased from 5 to 15 eV is due to the falling e^-–Rb spin transfer cross section.[22] The weak indication of polarization enhancement at 15 eV is attributable to the lowering of electron energies due to the onset of excitation of N_2 electronic states by the incident electrons, whereas the slow increase of P_e above E_i = 20 eV is caused by the increasing importance of slower ionized electrons from N_2 spin-exchanging with Rb atoms. At all incident energies, P_e is larger for the higher buffer gas pressure. The combined effects of thermalization of the electrons and a longer path length of these electrons through the polarized Rb due to the denser buffer gas explain this increase.

VII. A SIMPLE FIRST EXPERIMENT

With consistent performance of the device, we are using it as a source to study collisions of chiral (longitudinally polarized) electrons with chiral molecules. We have started by investigating the effect of electron handedness on the emission of secondary electrons from both enantiomers of cysteine. Electrons with a kinetic energy of 140 eV are incident on a layer of cysteine with thickness >150 nm deposited on a gold substrate. A negative bias on the gold drives the secondary electrons away from the surface after they are emitted. Keithley 6485 ammeters monitor the current incident on the biased

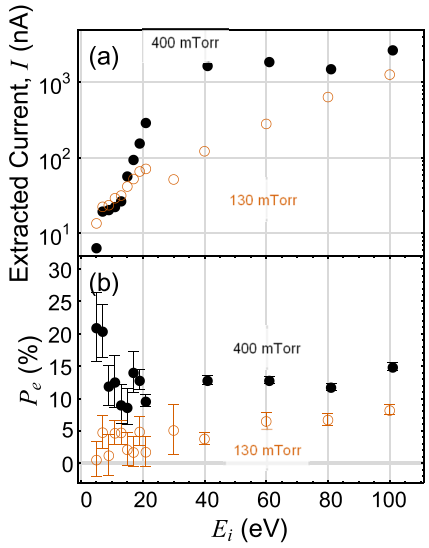

FIG. 18. The filled circles show the present performance of the apparatus, while the open circles, collected recently at $\mathcal{P}_{BG}$ = 130 mTorr, approximate the previous performance of the apparatus.[10] (a) Operating the system at $\mathcal{P}_{BG}$ = 400 mTorr resulted in improved values of P_e for all values of E_i. (b) The transmitted current was improved for intermediate energies but was slightly reduced for low and high values of E_i.

cysteine target. We observe a negative current corresponding to the incident electron beam current when the targets have a strong positive bias, and a positive current when the targets have zero or slightly negative bias, indicating the secondary electron emission current is greater than that of the incident beam. The experiment consists of alternating the helicity of the incident spin-polarized electrons and measuring the net current from the target in both cases. Then, we calculate the asymmetry in the current between the two measurements. Preliminary data collected in this manner are shown in Fig. 19.

Collecting the data in this way involves frequent changes in the targets, roughly every two days. With a standard GaAs source, this would require extended periods of downtime or a load-lock system, which would still not solve the problem of photocathode positioning. The Rb spin filter is particularly well suited for this task

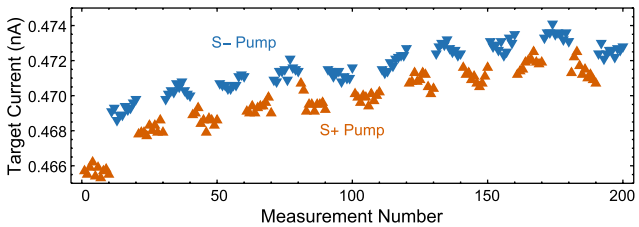

FIG. 19. Preliminary raw data searching for an asymmetry in secondary electron emission from cysteine. Although the data appear to have a large asymmetry, a significant portion of this is instrumental in nature. This figure simply illustrates the signal we analyze. The upward-pointing and downward-pointing symbols correspond to the two different helicities of the polarized electron beam.

because no bakeout period is needed after breaking vacuum, and data collection can begin within hours of loading a new target or Rb charge.

VIII. CONCLUSION AND FUTURE DIRECTIONS

The improved Rb spin filter produces beams of spin-polarized electrons even at vacuum pressures above 10^{-4} Torr. Electron polarizations above 20% can be consistently obtained with microamperes of current. Because the system operates at relatively high pressures, no bakeout procedure is needed after bringing the system to atmosphere, resulting in far less downtime than a typical GaAs source. The polarizations we have achieved in this work are the result of increasing the buffer gas pressure in the spin-exchange cell, made possible by the implementation of a turbomolecular pump on the source chamber and a differential pumping configuration. The device that was previously a proof-of-concept prototype has now advanced to the point of being used in a collision experiment.

Although reliable electron polarizations can be obtained with the current device, additional studies on how the buffer gas contributes to the electron polarization are needed to further improve its operation. Such studies could be carried out experimentally and complemented by Monte Carlo simulations.[23] Another beneficial modification would be a second differential pumping chamber immediately downstream from the Rb spin-exchange cell to reduce the detrimental effects of background buffer gases. Given the strong, longitudinal magnetic field in which the apparatus is immersed, the use of a trochoidal electron monochromator[12] to narrow the energy spread of the beam may also be implemented.

ACKNOWLEDGMENTS

This work was supported by NSF Award No. 2110358. The research was performed in part in the Nebraska Nanoscale Facility: National Nanotechnology Coordinated Infrastructure and the Nebraska Center for Materials and Nanoscience, which are supported by the National Science Foundation under Award No. ECCS: 2025298 and the Nebraska Research Initiative.

AUTHOR DECLARATIONS

Conflict of Interest

The authors have no conflicts to disclose.

Author Contributions

K. J. Ahrendsen: Conceptualization (equal); Data curation (equal); Software (equal); Writing – original draft (equal). **K. W. Trantham**: Conceptualization (equal); Funding acquisition (equal); Project administration (equal); Software (equal); Supervision (equal); Writing – review & editing (equal). **D. Tupa**: Conceptualization (equal); Software (equal); Writing – review & editing (equal). **T. J. Gay**: Conceptualization (equal); Funding acquisition (equal); Project administration (equal); Supervision (equal); Writing – review & editing (equal).

DATA AVAILABILITY

The data that support the findings of this study are available from the corresponding author upon reasonable request.

REFERENCES

[1]D. T. Pierce, F. Meier, and P. Zürcher, "Negative electron affinity GaAs: A new source of spin-polarized electrons," Appl. Phys. Lett. **26**, 670–672 (1975).

[2]J. M. Dreiling and T. J. Gay, "Chirally sensitive electron-induced molecular breakup and the vester-ulbricht hypothesis," Phys. Rev. Lett. **113**, 118103 (2014).

[3]F. C. Tang, M. S. Lubell, K. Rubin, A. Vasilakis, M. Eminyan, and J. Slevin, "Operating experience with a GaAs photoemission electron source," Rev. Sci. Instrum. **57**, 3004–3011 (1986).

[4]X. Q. Guo, D. M. Crowe, M. S. Lubell, F. C. Tang, A. Vasilakis, M. Eminyan, and J. Slevin, "Further observations on the operation of a GaAs polarized electron source," Rev. Sci. Instrum. **61**, 1858–1862 (1990).

[5]G. A. Mulhollan and J. C. Bierman, "Enhanced chemical immunity for negative electron affinity GaAs photoemitters," J. Vac. Sci. Technol., A **26**, 1195–1197 (2008).

[6]K. W. Trantham, "A search for electron circular dischroism in camphor," Ph.D. thesis, University of Nebraska-Lincoln, 1996, pp. 121–122, "We found that the typical 1/e lifetime of the GaAs electron source was reduced from ~3 days to ~8 h when camphor was present in the target chamber".

[7]A. S. Green, "Spin-dependent electron-molecule scattering," Ph.D. thesis, University of Nebraska-Lincoln, 2003, p. 183, "Longer data runs were not possible here because of bromocamphor contamination of the GaAs crystal. The crystal had to be heat cleaned and reactivated after each run, and this process took a day or two every time".

[8]J. M. Dreiling, "Asymmetric interactions between spin-polarized electrons and chiral molecules," Ph.D. thesis, University of Nebraska-Lincoln, 2014, p. 112 "Running at these lower pressures improved the crystal lifetime, although the GaAs photocathode photoemission still had a half-life of ~30 min".

[9]H. Batelaan, A. S. Green, B. A. Hitt, and T. J. Gay, "Optically pumped electron spin filter," Phys. Rev. Lett. **82**, 4216–4219 (1999).

[10]M. Pirbhai, J. Knepper, E. T. Litaker, D. Tupa, and T. J. Gay, "Optically pumped spin-exchange polarized-electron source," Phys. Rev. A **88**, 060701(R) (2013).

[11]M. Pirbhai, D. M. Ryan, G. Richards, and T. J. Gay, "Compact inline optical electron polarimeter," Rev. Sci. Instrum. **84**, 053113 (2013).

[12]A. Stamatovic and G. J. Schulz, "Characteristics of the trochoidal electron monochromator," Rev. Sci. Instrum. **41**, 423–427 (1970).

[13]K. W. Trantham, Piboard RS485, https://github.com/tranthamkw/piBoardRS485, 2021.

[14]Z. Wu, M. Kitano, W. Happer, M. Hou, and J. Daniels, "Optical determination of alkali metal vapor number density using Faraday rotation," Appl. Opt. **25**, 4483 (1986).

[15]D. A. Steck, Rubidium 87 D line data, available online at http://steck.us/alkalidata; revision 2.2.3, 9 July 2021.

[16]A. Ueno, K. Takasaki, K. Ogura, Y. Wakuta, I. Kumabe, K. O-Ohata, Y. Mori, and S. Fukumoto, "Faraday rotation of optically pumped sodium vapour in a weak magnetic field," Nucl. Instrum. Methods Phys. Res., Sect. A **262**, 170–178 (1987).

[17]E. B. Norrgard, D. Tupa, J. M. Dreiling, and T. J. Gay, "Electron-spin-reversal phenomenon in optically pumped rubidium," Phys. Rev. A **82**, 033408 (2010).

[18]M. A. Rosenberry, J. P. Reyes, D. Tupa, and T. J. Gay, "Radiation trapping in rubidium optical pumping at low buffer-gas pressures," Phys. Rev. A **75**, 023401 (2007).

[19]H. G. Berry, G. Gabrielse, and A. E. Livingston, "Measurement of the Stokes parameters of light," Appl. Opt. **16**, 3200 (1977).

[20]T. J. Gay, "A simple optical electron polarimeter," J. Phys. B: At. Mol. Phys. **16**, L553–L556 (1983).

[21]Y. Itikawa, "Cross sections for electron collisions with nitrogen molecules," J. Phys. Chem. Ref. Data **35**, 31–53 (2006).

[22]C. Bahrim, U. Thumm, and I. I. Fabrikant, "Negative-ion resonances in cross sections for slow-electron–heavy-alkali-metal-atom scattering," Phys. Rev. A **63**, 042710 (2001).

[23]K. J. Ahrendsen, W. J. Brunner, and T. J. Gay, "Studies of collision dynamics in Rb spin-exchange cells," in APS Division of Atomic And Molecular Physics Meeting 2019, 2019, Abstract ID No. E01.020.